To be published in Optics Express:

Title: Sub-micron picoplankton shape, orientation and internal structure combine to preferentially amplify forward scatter

Authors: Timothy Smyth,Glen Tarran,Shubha Sathyendranath

Accepted: 22 December 20

Posted 22 December 20

DOI: https://doi.org/10.1364/OE.413576

Sub-micron picoplankton shape, orientation and internal structure combine to preferentially amplify forward scatter

T. J. SMYTH,[1,*] G. A. TARRAN,[1] AND S. SATHYENDRANATH[1]

[1]*Plymouth Marine Laboratory, Prospect Place, Plymouth, Devon, PL1 3DH, UK*
**tjsm@pml.ac.uk*

Abstract: Compelling evidence is presented that sub-micron picoplankton shape, internal structure and orientation in combination leads to a disproportionate enhancement of differential forward scatter compared with differential side scatter when analyzed with a flow cytometer. Theoretical evidence is provided which results in an order of magnitude amplification in the forward scatter direction, with little or no change in the side scatter: this discounts the possibility of "doublets" caused by multiple particles simultaneously present in the laser beam. Observational evidence from progressively finer filtered seawater samples shows up to three orders of magnitude enhancement in the forward scatter direction and sizes of *Prochlorococcus* close to that reported in the literature (0.61±0.17μm). It therefore seems likely that flow cytometrically observed "bi-modal size distributions" of *Prochlorococcus* are instead the manifestation of intra-population differences in shape (spherical – prolate with preferential alignment) and internal structure (homogenous – heterogenous).

1. Introduction

In our recent extensive flow cytometric analysis [1] of the variability of natural assemblages of marine picoplankton, in particular *Prochlorococcus* [2] and *Synechococcus* [3, 4], we demonstrated that *Prochlorococcus* frequently showed double size distribution peaks, on average (N~10^4 samples) centred on 0.75±0.25 and 1.75±0.25 μm; smallest peak diameters were ≤0.65 μm in the equatorial upwelling with larger cells (~0.95 μm) in the surface layers of the tropical gyres. We also put forward the idea of "opto-types" where different parts of the double size distribution peaks in *Prochlorococcus* dominated at different depths and in different provinces of the Atlantic Ocean. The term "opto-type" was coined as the two populations had distinctive side- and forward- scatter characteristics which when inverted using Mie scattering calculations resulted in the smaller having a higher refractive index than the larger sized cells. These observations were qualitatively consistent with previously-known ecotypes [5-7] of *Prochlorococcus* with distinct adaptions to environmental factors such as light intensity, temperature and nutrient concentrations [8], as well as remarkable genetic and physiological diversity [5].

On a subsequent Atlantic Meridional Transect cruise (AMT29) we put these ideas to further scrutiny by taking successively finer filtered samples, and analysing them using a flow cytometer, so that we could manually, as well as automatically, control the size distribution in order to validate our automatically determined size distribution results and methodology. However, we have found a discrepancy between the size fractionated and the flow cytometrically derived sizes. When the samples were filtered through filters with pore sizes ≤ 2μm, the scattering inversion calculations which depend on Mie theory [9, 10], were "detecting" a sizeable fraction of particles (~50% of the total) in excess of 4 μm. In this article we look at two potential sources of the artefact: (1) inadequacies in the particle scattering calculation assumptions and (2) possible issues caused by sub-micron particles within the flow cytometer itself.

2. Method

2.1 Size fractionated in situ measurements

Seawater samples were collected at 24 stations on the Atlantic Meridional Transect research cruise (AMT29) between 20 October and 18 November 2019 for successive size fractionated analyses. The individual samples were collected from Niskin bottles attached to a Sea-bird Electronics (Washington, USA) oceanographic rosette sampler into clean 250 mL polycarbonate bottles (Nalge Company, USA)

at a single depth within the top mixed layer or close to the deep chlorophyll maximum. These were then stored at 4°C in the dark and analysed within two hours.

Size fractionated samples were prepared by gravity filtering 4 mL seawater samples through 47 mm diameter Whatman™ Nuclepore™ polycarbonate membrane filters within Sartorius in-line polycarbonate filter housings held vertically in a burette stand, with flow cytometry tubes below to retain the filtrates. Filters of pore sizes 0.2, 0.4, 0.6, 0.8, 1, 2, 3, 5, 8 and 10 µm were used to produce the filtrates which were then analysed, along with an unfiltered sample using a Becton Dickinson FACSort™ flow cytometer.

Two types of numerical analysis were carried out: (i) manually gated enumerated abundances [11] of *Prochlorococcus* and *Synechococcus* (as well as nanophytoplankton) for successively smaller filter pore sizes were used to determine the size at which 50% (median) of the original unfiltered population abundance remained; (ii) the automatic clustering technique of Smyth, et al. [1] was applied to the flow cytometry data from the different filter pore sizes for each sample to simultaneously calculate cell size and abundance. In brief the calculation of size and refractive index is achieved by using the calibrated forward and side scatter flow cytometric measurements [12] to calculate the differential forward scatter ($dC_{sca}/d\Omega_3$) and differential side scatter ($dC_{sca}/d\Omega_4$) [10]. This scattering pair is then used within a look-up-table [1] to determine size and refractive index.

2.2 Scattering calculations

For the purposes of scattering calculations it is widely assumed that the smallest phytoplankton are well described as homogenous spheres [1, 12-14] and therefore adhere closely to Mie theory [9, 10]. Observed departures from Mie scattering theory may be caused by changes in particle shape [15] and internal structure [16]; additionally, once a particle is no longer spherical, its orientation [17] within the flow cytometer laser beam may significantly change the received scattering signal pair ($dC_{sca}/d\Omega_3$; $dC_{sca}/d\Omega_4$). Taken in isolation, each of these factors have been previously considered to be relatively small [1] or amplify the backscatter cf. forward scatter [16]. Here, for the first time, we consider all these factors in combination using scattering calculations based on the Extended Boundary Condition Method (EBCM) made available in the Python programming language as the package ScattPy [18]. We assumed that the particles were all prolate spheroids (oblate spheroids are "…a rather unlikely shape for phytoplankton" [19]) and that they were simplistically made up of two layers [16] of different refractive index (n), comprising of a thin outer shell, of refractive index n_1, and larger inner core of refractive index n_2 such that $n_1 > n_2$ (shell > core). The orientation angle (α) is defined as being parallel to the major axis of the prolate spheroid [15].

In order to determine the general enhancement of scattering by particles of different shapes, sizes, compositions and orientations, the scattering efficiency (Q_{sca}[10]), which is defined as the ratio of the scattering cross section (C_{sca}) to the geometric cross section (A), was calculated using the Scattpy [18] code. The experiments, all as a function of axial ratio (1.0, 1.5, 2.0, 3.0) and particle size, were as follows: (1) homogenous prolate spheroids with fixed n (1.06) and orientation (α=0°); (2) coated prolate spheroids with the default values for n_2, n_1 and outer shell volume being 1.06, 1.13 and 17% respectively [16] and fixed orientation (α=0°); (3) as for (2) but orientation fixed at α=45°; (4) as for (2) but orientation fixed at α=90°. The particle width (minor axis dimension) range maximum of 0.6 µm was selected on the basis that cells of this size would represent the maximum size permitted through 0.6 µm filter pores: 0.6 µm was the size closest to that determined (see Table 1) by the manually gated analysis (0.61 µm) and is also consistent with previous literature values for the size of *Prochlorococcus* (0.5 – 0.7 µm [8]).

A similar approach was taken in order for the modelled scattering patterns to have direct applicability to the flow cytometer observation pairs of ($dC_{sca}/d\Omega_3$; $dC_{sca}/d\Omega_4$). Four scattering calculation experiments were carried out at three different particle orientation angles (α=0, 45, 90°) with the default values for n_2, n_1 and outer shell volume being 1.06, 1.13 and 17% respectively at a default axial ratio of 1.5 and minor axis width of 0.6 µm. The experiments were: (1) variable axial ratio (range: 1.0 – 2.5); (2) variable n_1 (range: 1.10 – 1.20); (3) variable n_2 (range: 1.02 – 1.08) and; (4) variable shell volume (range: 1 – 20% of the whole particle).

3. Results

3.1 In-situ size fractionated

Date	Lat (°N)	Lat (°E)	Depth (m)	*Pro* Auto (N)	*Pro* gated (N)	*Pro* diameter (µm)
20/10/19	42.24	-19.20	20	30513	33555	0.63

21/10/19	40.18	-21.93	**55**	44381	54110	0.60
23/10/19	35.89	-26.88	20	***5490***	13127	0.52
24/10/19	33.18	-29.33	**92**	9627	11459	0.71
26/10/19	28.76	-33.03	30	***1760***	11444	0.43
27/10/19	26.14	-35.19	**115**	11428	13644	0.63
28/10/19	23.42	-37.53	**124**	9417	13307	0.73
30/10/19	18.06	-32.97	75	83962	90264	0.54
31/10/19	15.59	-30.43	27	75959	96805	0.53
02/11/19	9.88	-26.79	**46**	***37821***	23719	0.88
03/11/19	6.75	-25.00	21	***1323***	10944	0.50
04/11/19	2.88	-24.99	**70**	52690	57627	0.54
06/11/19	-4.30	-25.00	40	***2446***	10930	0.52
07/11/19	-7.39	-25.01	**90**	34834	41956	0.70
08/11/19	-10.67	-25.00	43	***1777***	10291	0.70
09/11/19	-14.27	-24.99	**150**	66633	71157	0.53
11/11/19	-20.25	-25.00	92	***7358***	21575	0.71
12/11/19	-23.73	-24.92	**168**	56011	60776	0.54
13/11/19	-26.76	-25.81	51	***9939***	26760	0.51
14/11/19	-30.03	-26.79	**110**	45484	51022	0.58
15/11/19	-33.60	-27.89	25	***429***	5096	0.50
16/11/19	-37.08	-29.02	**55**	***2547***	9224	0.58
17/11/19	-40.36	-31.04	**40**	***104***	483	0.94
						0.61±0.17

Table 1. Size fractionated determined median size *Prochlorococcus* (*Pro*) for 23 (out of 24) experiments along the AMT29 transect. Abundances for gated (*Pro* gated) results are shown as well as the automated clustering approach (*Pro* auto). Depths in bold are situated in or just above the sub-surface chlorophyll maximum. Bold italicized automated clustering abundances are where there is more than 30% deviation from the gated results.

Table 1 shows the size fractionated results for the manually gated and automated enumeration (for *Prochlorococcus* only, see Table A1 for full results): the average median size for *Prochlorococcus* is 0.61±0.17µm. These values for *Prochlorococcus* are closer to the literature values of 0.5 – 0.7 µm in diameter [8] than those reported in Smyth, et al. [1] where the typical peak sizes for Prochlorococcus varied between 0.65 (equatorial upwelling, ~120 m) and 0.95 µm (centre of the north and south Atlantic gyres). What is also not apparent in the manually gated size fractionated data is a bi-modal distribution.

3.2 Automated size classification

This lack of a bi-modal distribution, or double peak, caused us to look in more detail at the automated classification data. It is important to note that the automated classification of type (*Prochlorococcus*) and hence abundance is reliant only upon differential side scatter ($dC_{sca}/d\Omega_4$) and red fluorescence (Fig. 1A. and B.). The pairing of ($dC_{sca}/d\Omega_3$; $dC_{sca}/d\Omega_4$) is as a result of this set determined by the automated classifier i.e. $dC_{sca}/d\Omega_3$ does not determine the type, once the type is determined, the size (and refractive index) is retrievable from the observed ($dC_{sca}/d\Omega_3$; $dC_{sca}/d\Omega_4$) pair. Although the automated cluster enumerated abundance flow cytometer data is generally within 30% of the manual gating (Table 1), when the differential forward scatter, ($dC_{sca}/d\Omega_3$), is plotted against the differential side scatter, ($dC_{sca}/d\Omega_4$) for the same sample but unfiltered (Fig. 1A,C) and 0.6 µm filtered (Fig. 1B,D), it becomes clear that the scattering inversion to derive size and refractive index has become compromised for these sub-micron phytoplankton (Fig. 1D).

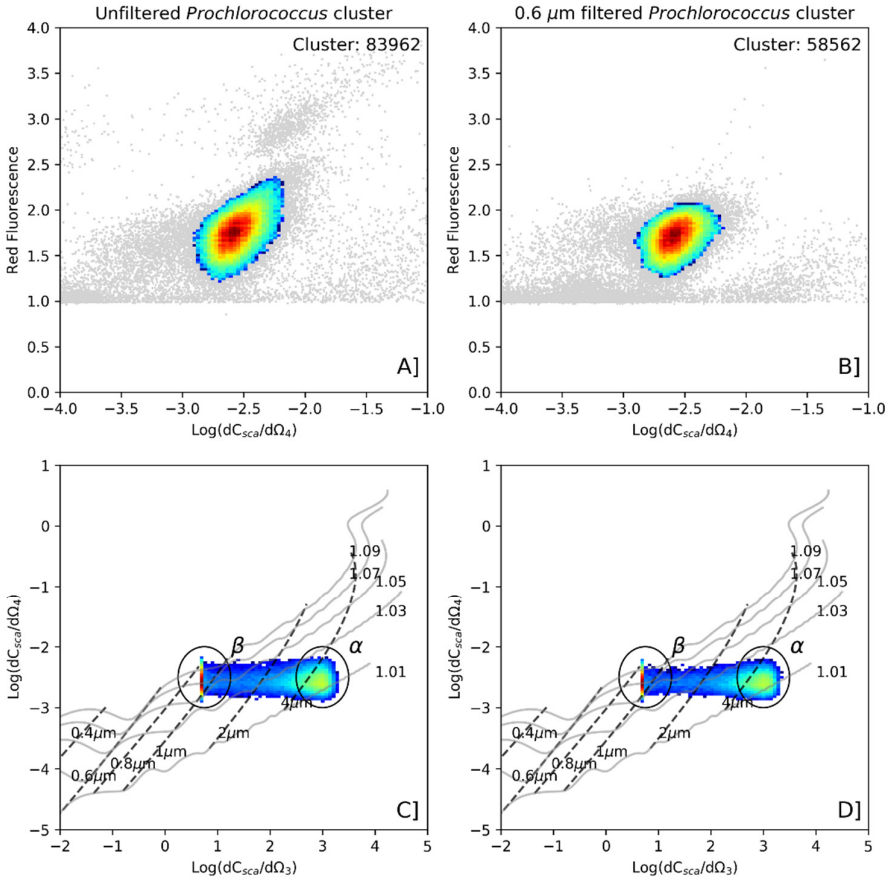

Fig. 1: Automatic clustering technique [1] for *Prochlorococcus* for unfiltered A] and 0.6 µm filtered B] sample taken on 30 October 2019 (18.06°N; 32.97°W depth=75m) – see Table 1 row 8. The equivalent side vs. forward log differential scatter ($dC_{sca}/d\Omega_4$ vs. $dC_{sca}/d\Omega_3$) plots for unfiltered C] and 0.6 µm filtered D] with theoretically calculated [1] contours of equal diameter (dashed: 0.4, 0.6, 0.8, 1, 2 and 4µm) and refractive index (solid: 1.01, 1.03, 1.05, 1.07, 1.09). Regions circled as α, β in C] and D] show a bi-modal distribution; in D] both regions should be unpopulated.

This is shown in regions α and β in Fig. 1D. Region α is showing *Prochlorococcus* with an apparent (according to scattering inversion calculation [1]) diameter of 2 – 4.5 µm; region β an apparent diameter between 0.8 and 1 µm. Both α and β, for both the unfiltered (Fig. 1C) and filtered (Fig. 1D) sample, contain about 50% of the population abundance; the denser distribution in β being a function of an apparently smaller size range (0.2 µm cf. 2.5 µm). However, in region β the instrument is simply assigning the limit of detection (LoD) value to $dC_{sca}/d\Omega_3$ for cells it can measure no meaningful forward scattering for. The straight-line feature at the LoD is caused by variability in $dC_{sca}/d\Omega_4$, mainly driven by changes in the cell refractive index.

This raises the question as to what is causing the data artefact in region α, and indeed the continuum linking regions α and β, because of the physical impossibility of getting 0.8 – 4.5 µm diameter phytoplankton cells through 0.6 µm filter pores. It is clear from Fig. 1D that most of the scattering amplification is in the forward (x-axis) rather than the side (y-axis) scatter direction. There are >3 orders of magnitude difference between the scattering theory predicted ($\log(dC_{sca}/d\Omega_3) \sim 3$) and what should be expected for a spherical, homogenous particle of D=0.6 µm and n=1.06 ($\log(dC_{sca}/d\Omega_3) \sim -0.7$).

3.3 Particle scattering calculations

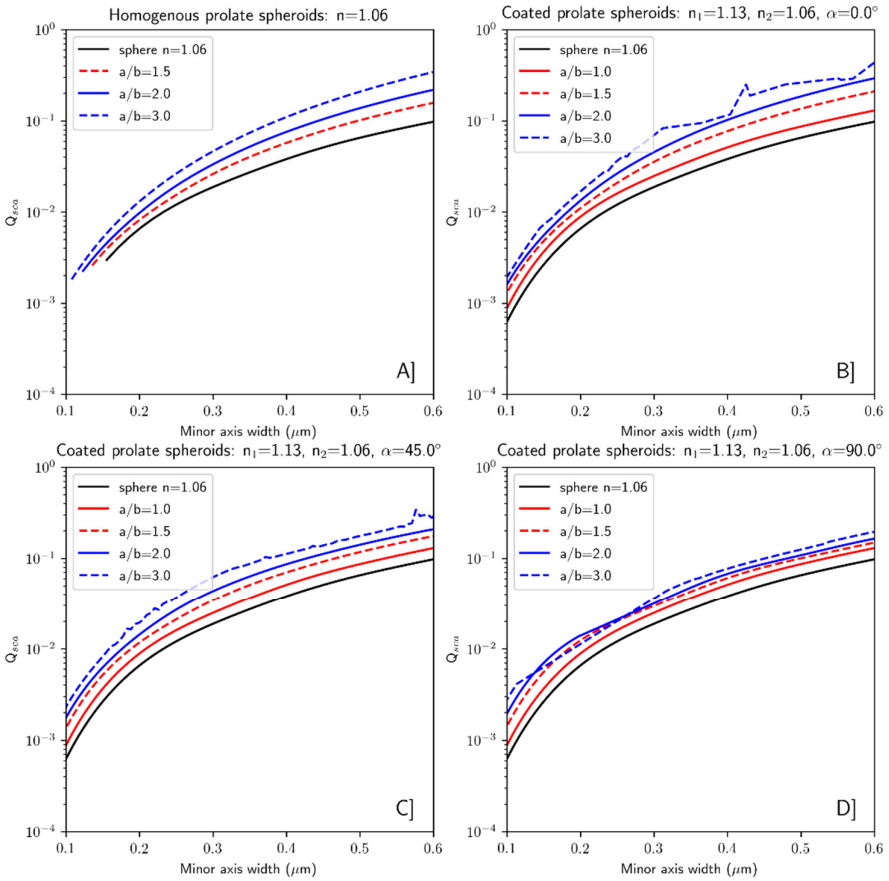

Fig. 2: Scattering efficiency (Q_{sca}) for particles of variable size, shape, internal structure and orientation. A] Homogenous prolate spheroid (n=1.06) for range of axial ratios (a/b) plotted as a function of the particles' minor axis width [15]; B] Coated prolate spheroid with outer shell n_1=1.13, inner core n_2=1.06 at a beam incident angle α=0° for range of a/b. Volume of outer shell is 17% of total [16]; C] as B] but for α=45°; D] as B] but for α=90°.

Fig. 2 shows that the combination of shape, internal structure and beam incidence angle increases the scattering efficiency (Q_{sca} [10]) by up to a factor of six for a particle of minor axis = 0.6 µm and axial ratio = 3.0 compared with a spherical homogenous particle with D = 0.6 µm. The values of n_1 (=1.13) and n_2 (=1.06), together with the shell volume (17%) were chosen for consistency with previous values in the literature [16]. The greatest scattering amplification is when the incidence angle of the beam, α, is 0° (Fig. 2B), i.e. parallel to the long-axis of the particle; this is progressively diminished for increasing values of α (Fig. 2C,D).

The value of Q_{sca} is a measure of the integrated volume scattering function: in this work we are interested in the differential forward and side scattering ($dC_{sca}/d\Omega_3$; $dC_{sca}/d\Omega_4$) in order to calculate the signals measured by the flow cytometer detectors [1, 12-14]; the forward scatter detector collects light between 1±12.2° and the side detector between 64 - 116° [1].

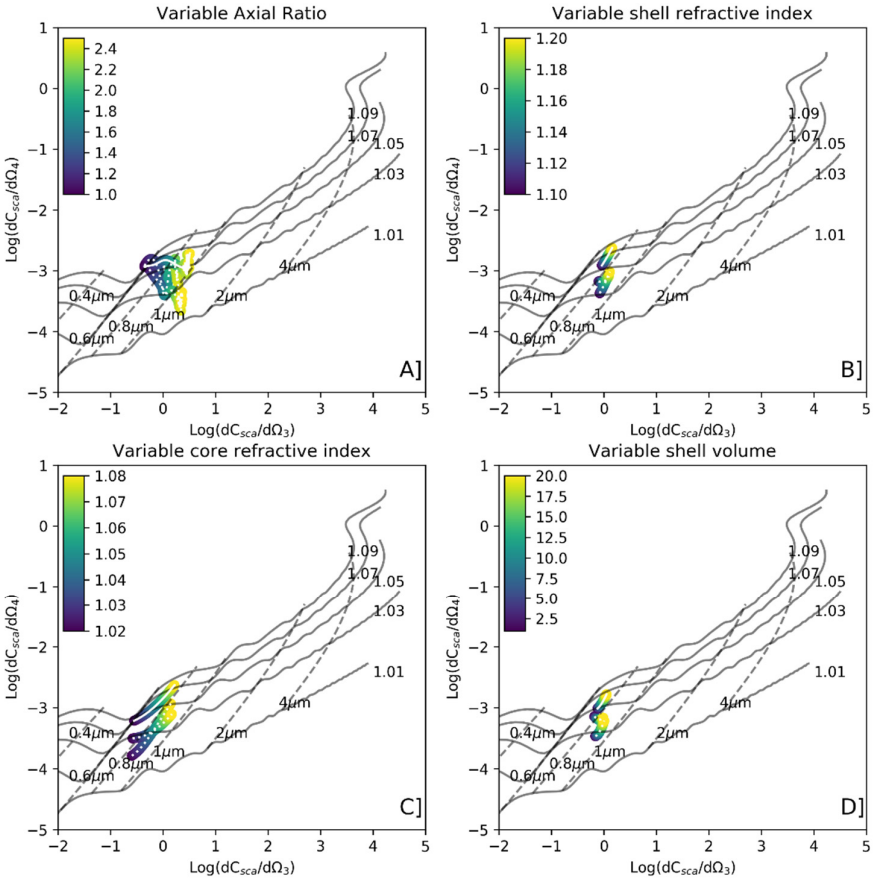

Fig. 3: Modelled prolate spheroid results for A] variable axial ratio; B] variable n_1; C] variable n_2 and D] variable shell volume, whilst keeping the remaining variables fixed at different angles of incidence (α=0° (white solid), 45° (white dotted), 90° (white dotted)). All overlaid onto Mie theory modelled values of size (long dashed: range 0.4 μm – 4 μm) and n (solid: range 1.01 – 1.09) as a function of differential forward ($dC_{sca}/d\Omega_3$) and side ($dC_{sca}/d\Omega_4$) scatter modelled for a flow cytometer [1] of known internal geometry.

Fig. 3A clearly shows that an order of magnitude increase in $dC_{sca}/d\Omega_3$ can theoretically be achieved when comparing a homogenous sphere (D=0.6μm, n=1.06) with a two-layered prolate spheroid (axial ratio=2.5; minor axis=0.6μm; n_1=1.13; n_2=1.06; shell volume=17%), with only a small change in $dC_{sca}/d\Omega_4$ when α=0°. In other words, such a two-layered prolate spheroid has near identical scattering characteristics ($dC_{sca}/d\Omega_3$; $dC_{sca}/d\Omega_4$) of a Mie particle (homogenous sphere) with D=1μm, n=1.05. Although Fig. 3B-D shows an increase in $dC_{sca}/d\Omega_3$ for increasing n_1, n_2 and shell volume respectively, there is also a similar (Fig. 3C) or greater (Fig. 3B,D) increase in $dC_{sca}/d\Omega_4$ which is not consistent with the scattering patterns shown in Fig. 1D.

4. Discussion

The scattering calculations present compelling evidence that particle shape, internal structure and orientation in combination leads to an enhancement of the differential forward scatter, with a smaller change in the differential side scatter. The changes in axial ratio in particular are key to understanding this behavior and the invalidation of the Mie scattering assumptions made for interpreting the flow cytometer scattering signal. However, the scattering calculations carried out in order to explain region α in Fig. 1D can only account for an order of magnitude enhancement (O1) in $dC_{sca}/d\Omega_3$; whereas an O3 increase is required to replicate the observations.

Sub-micron particles are known to cause issues for flow cytometers in medical applications [20] with the generation of "doublets" (see Fig. 1 of Hobson and Sims [20]). This is caused by aggregation of particles and, as a consequence, more than one particle being in the laser beam at any given moment. This causes an overestimation in the particle side and forward scatter. This in turn will cause an overestimation in the particle size, and in our application, a different refractive index will result from the inversion scheme. This effect is further exacerbated by the flow cytometer necessarily being calibrated against polystyrene beads [20] which have different optical properties (primarily refractive index but also size) to the target samples (picoplankton).

A counter argument to the "doublet" explanation of the data shown in Fig. 1D is there is only an increase in $dC_{sca}/d\Omega_3$, whereas $dC_{sca}/d\Omega_4$ remains relatively unchanged: when doublets are observed there is an increase in the signal detected in both directions [20]. The presence of doublets in the data would also call into question the ability of flow cytometers to accurately enumerate sub-micron phytoplankton such as *Prochlorococcus*. A further analysis (not shown here) concluded that the side scatter signal was more coherently clustered than the forward scatter signal for the sample shown in Fig. 1, and more generally for the samples summarized in Table 1. This would further lend weight to dismissing the doublet explanation and favouring the combination of shape and internal structure of the individual cells amplifying the forward scatter signal.

Although region α in Fig. 1D gives most cause for concern, region β also causes problems: the gain setting for the forward scatter channel on the flow cytometer has historically been set too low to register the smallest particles' forward scatter correctly; this is not the case for the side scatter. This is because, up until now, the manually gated enumeration technique did not require forward scatter for cell discrimination. Consequently the extent of $dC_{sca}/d\Omega_3$ is registered at the LoD (left-right direction), but there is still variability in $dC_{sca}/d\Omega_4$ (up-down direction). This has the effect of showing more variability in refractive index than in size because of the relative orientation of the refractive index and size contours: size is a stronger function of forward scatter; refractive index is a stronger function of side scatter.

Intriguingly, recent modelling results for the flow cytometric signature of human red blood cells [17] have shown that experimentally observed bi-modal distributions can be explained by shape elongations caused by hydrodynamic forces within the flow cytometer. They also concluded that biological variations of cell size and intracellular hemoglobin concentration (i. e., variable refractive index, n) turn out to have effects of similar magnitude as the change in shape.

The question therefore remains: is the scattering pattern shown in Fig. 1D, clearly showing a bi-modal size distribution, entirely an artefact caused by the flow cytometer itself? Or is there sufficient evidence within the scattering patterns to support our previous assertions regarding "opto-types"[1]? Bi-modal size distributions of *Prochlorococcus* are presented in the literature [21] and the internal structural complexity of *Prochlorococcus* is apparent from transmission electron microscopy imagery (e.g. Fig. 2 in Bryant [22]) as well as its departure from sphericity [8]. It is likely therefore that the scattering calculations presented here do not replicate the precise patterns observed in Fig. 1D because the complexities of shape, orientation and internal structure defy calculation tractability: the number of layers, their individual refractive indices, the angular orientation of the particle and even the presence of gas vacuoles [23] within the *Prochlorococcus* cell all in combination would require a large number of individual calculations to cover all permutations and combinations. Although there is a continuum of likely cell characteristics (shape, structure, composition) and behaviours (orientation) between regions α and β in Fig. 1D it is still the case that there is a stark division between the two – almost as if there is a preferred or favoured size, shape, composition and orientation combination. However, because of the computational limitation and indeed the stability of the scattering calculations themselves we have not been able to fully explain this.

We hypothesize therefore that the scattering pattern shown in Fig. 1D is as a result of a bi-modal scattering distribution, not necessarily caused by size, but dominated by shape and structure. Region β is populated by cells which can accurately be described using Mie theory as homogenous spheres, the retrieval of the precise size and refractive index being stymied by the low gain setting on the flow cytometer. Region α, although giving the forward and side scatter characteristics equivalent to a Mie particle ($D \approx 2.5 - 4.5\mu m$; $n \approx 1.03$) in reality comprises of prolate cells, of preferred angular orientation within the laser beam and have a complex internal structure.

Finally, the question remains on how we can use these results to improve our flow cytometer measurement method [1]. Simply inspecting Fig. 1D it would seem immediately obvious that the LoD for $\log(dC_{sca}/d\Omega_3)$ needs to be reduced to around -1.0 (from 0.7) in order to detect the forward scatter for such small particles in region β, but there are inherent technical difficulties in achieving this including reducing the signal to noise ratio of the instrument. This paper has also highlighted the vast complexity of *Prochlorococcus* cells in the real-world environment and there is still the need to further

develop computer code which can stably, accurately and efficiently model their scattering characteristics when they depart from sphericity and homogeneity. As the automated classification sub-micron phytoplankton such as *Prochlorococcus* is relatively robust [1], relying as it does upon side scatter and red fluorescence [11], there may be artificial intelligence / machine learning approaches [24] which may enable the accurate retrieval of the forward scatter signal, and the subsequent determination of the cell size and composition.

4. Conclusions

The automated clustering technique described in Smyth, et al. [1] generally works well for the enumeration of *Prochlorococcus* and can detect successively fewer cells passing through successively finer filter pore sizes. This is because the clustering technique uses well characterized fluorescence and differential side scatter data. However, the determination of size and refractive index, which is a function of differential forward and differential side scatter, has been called into question for these sub-micron phytoplankton.

We have shown that the shape of sub-micron *Prochlorococcus* cells in concert with their internal structure and preferred angular orientation, can lead to substantial changes to the scattering patterns measured by a flow cytometer. Additionally, low sensitivity used in the forward scatter channel of a flow cytometer, doesn't allow these sub-micron particles to be attributed the correct value of differential forward scatter. Instead these particles give a signal in the differential side scatter direction and appear at the LoD for the differential forward scatter. Therefore conclusions reached in Smyth, et al. [1] about the size distribution and refractive index of *Prochlorococcus* will likely need revising in the light of these data. The average peaks in the bi-modal size distribution reported [1] of 0.75±0.25 and 1.75±0.25 μm are likely an overestimate: the lower peak because the forward scatter signal is assigned to the LoD of the flow cytometer and the upper peak because, as we have shown here with size fractionated samples, a similar feature exists when the filter pore diameter should preclude cells of this size passing through. We hypothesize therefore, based on the result of this paper, that this apparent bi-modality is caused by the simultaneous presence of (1) sub-micron *Prochlorococcus* cells being well characterized by Mie scattering theory (spherical and homogenous) and (2) sub-micron prolate spheroid *Prochlorococcus* cells with complex internal structure, preferentially aligned within the flow cytometer.

Funding

This work was funded by the UK Natural Environment Research Council through its National Capability Long-term Single Centre Science Programme, Climate Linked Atlantic Sector Science, grant number NE/R015953/1, and is a contribution to the Atlantic Meridional Transect and Theme 1.3 – Biological Dynamics. This work was supported by the Simons Collaboration on Computational Biogeochemical Modeling of Marine Ecosystems/CBIOMES (Grant ID: 549947,SS).

Acknowledgements

This study contributes to the international IMBeR project and is contribution number # of the AMT programme.

Disclosures

The authors declare no conflicts of interest.

Appendix

Date	Lat (°N)	Lat(°E)	Depth (m)	Syn (N)	Syn diameter (μm)	Pro (N)	Pro diameter (μm)	Pro Auto (N)	Nano diameter (μm)
20/10/19	42.24	-19.20	20	442	0.95	33555	0.63	30513	2.70
21/10/19	40.18	-21.93	**55**	650	0.97	54110	0.60	44381	3.25
23/10/19	35.89	-26.88	20	261	0.88	13127	0.52	5490	5.14
24/10/19	33.18	-29.33	**92**	22	1.00	11459	0.71	9627	4.00
26/10/19	28.76	-33.03	30	211	0.78	11444	0.43	1760	6.12
27/10/19	26.14	-35.19	**115**	23	0.98	13644	0.63	11428	-
28/10/19	23.42	-37.53	**124**	10	-	13307	0.73	9417	-
30/10/19	18.06	-32.97	75	831	0.93	90264	0.54	83962	2.70

31/10/19	15.59	-30.43	27	5274	0.88	96805	0.53	75959	5.43
02/11/19	9.88	-26.79	**46**	3297	0.93	23719	0.88	37821	3.87
03/11/19	6.75	-25.00	21	486	0.78	10944	0.50	1323	3.85
04/11/19	2.88	-24.99	**70**	942	0.96	57627	0.54	52690	5.23
06/11/19	-4.30	-25.00	40	70	0.90	10930	0.52	2446	3.90
07/11/19	-7.39	-25.01	**90**	121	1.42	41956	0.70	34834	2.70
08/11/19	-10.67	-25.00	43	166	0.80	10291	0.70	1777	3.90
09/11/19	-14.27	-24.99	**150**	95	0.72	71157	0.53	66633	4.00
11/11/19	-20.25	-25.00	92	228	1.00	21575	0.71	7358	3.95
12/11/19	-23.73	-24.92	**168**	109	0.93	60776	0.54	56011	3.95
13/11/19	-26.76	-25.81	51	377	0.85	26760	0.51	9939	3.95
14/11/19	-30.03	-26.79	**110**	153	1.18	51022	0.58	45484	-
15/11/19	-33.60	-27.89	25	175	0.73	5096	0.50	429	4.84
16/11/19	-37.08	-29.02	**55**	11807	0.96	9224	0.58	2547	1.76
17/11/19	-40.36	-31.04	**40**	67820	0.90	483	0.94	104	-
18/11/19	-41.90	-35.43	10	2245	1.25	-	-	8	2.10
					0.94±0.16		**0.61±0.17**		**3.87±1.04**

Table A2. Size fractionated determined median size for *Synechococcus* (Syn) , *Prochlorococcus* (Pro) and other nano phytoplankton (Nano) [1] for 24 experiments along the AMT29 transect. Abundances for gated results are shown as well as the automated clustering approach for Pro. Depths in bold are situated in or just above the sub-surface chlorophyll maximum.

The average median size for *Synechococcus* (0.94±0.16µm) are close to those previously reported in the literature[3], where they have been variously described as coccoid to rod-shaped, 0.7 to 0.9µm in diameter and 1.25 – 2.5µm in length. In Smyth, et al. [1] the sizes reported vary between 1.50 (surface South Atlantic Gyre) and 2.75 µm (at depths >150 m). For the purposes of inter-comparison with the automated technique [1] *Synechococcus* cells are at generally insufficient concentrations (<1000) in order to generate meaningful statistics.

References

1. T. J. Smyth, G. A. Tarran, and S. Sathyendranath, "Marine picoplankton size distribution and optical property contrasts throughout the Atlantic Ocean revealed using flow cytometry," Applied Optics **58**, 8802-8815 (2019).
2. S. W. Chisholm, R. J. Olson, E. R. Zettler, R. Goericke, J. B. Waterbury, and N. A. Welschmeyer, "A novel free-living prochlorophyte abundant in the oceanic euphotic zone," Nature **334**, 340-343 (1988).
3. J. B. Waterbury, S. W. Watson, R. R. L. Guillard, and L. E. Brand, "Widespread occurrence of a unicellular, marine, planktonic, cyanobacterium," Nature **277**, 293-294 (1979).
4. P. W. Johnson and J. M. Sieburth, "Chroococcoid cyanobacteria in the sea - ubiquitous and diverse phototropic biomass," Limnology and Oceanography **24**, 928-935 (1979).
5. G. Rocap, F. W. Larimer, J. Lamerdin, S. Malfatti, P. Chain, N. A. Ahlgren, A. Arellano, M. Coleman, L. Hauser, W. R. Hess, Z. I. Johnson, M. Land, D. Lindell, A. F. Post, W. Regala, M. Shah, S. L. Shaw, C. Steglich, M. B. Sullivan, C. S. Ting, A. Tolonen, E. A. Webb, E. R. Zinser, and S. W. Chisholm, "Genome divergence in two Prochlorococcus ecotypes reflects oceanic niche differentiation," Nature **424**, 1042-1047 (2003).
6. J. W. Chandler, Y. J. Lin, P. J. Gainer, A. F. Post, Z. I. Johnson, and E. R. Zinser, "Variable but persistent coexistence of Prochlorococcus ecotypes along temperature gradients in the ocean's surface mixed layer," Environmental Microbiology Reports **8**, 272-284 (2016).
7. E. R. Zinser, A. Coe, Z. I. Johnson, A. C. Martiny, N. J. Fuller, D. J. Scanlan, and S. W. Chisholm, "Prochlorococcus ecotype abundances in the North Atlantic Ocean as revealed by an improved quantitative PCR method," Appl. Environ. Microbiol. **72**, 723-732 (2006).
8. F. Partensky, W. R. Hess, and D. Vaulot, "Prochlorococcus, a marine photosynthetic prokaryote of global significance," Microbiology and Molecular Biology Reviews **63**, 106-+ (1999).
9. G. Mie, "Contribution to the optical properties of turbid media, in particular of colloidal suspensions of metals," Ann. Phys. (Leipzig) **25** 377 – 452 (1908).
10. C. F. Bohren and D. R. Huffman, *Absorption and scattering of light by small particles* (Wiley, New York, 1983).
11. G. A. Tarran, J. L. Heywood, and M. V. Zubkov, "Latitudinal changes in the standing stocks of eukaryotic nano- and picophytoplankton in the Atlantic Ocean," Deep-Sea Research II **53**, 1516 - 1529 (2006).
12. S. G. Ackleson and R. W. Spinrad, "Size and refractive-index of individual marine particulates - a flow cytometric approach," Applied Optics **27**, 1270-1277 (1988).
13. R. E. Green, H. M. Sosik, R. J. Olson, and M. D. DuRand, "Flow cytometric determination of size and complex refractive index for marine particles: comparison with independent and bulk estimates," Applied Optics **42**, 526-541 (2003).
14. J. Agagliate, R. Rottgers, M. S. Twardowski, and D. McKee, "Evaluation of a flow cytometry method to determine size and real refractive index distributions in natural marine particle populations," Applied Optics **57**, 1705-1716 (2018).

15. S. Asano, "Light-scattering properties of spheroidal particles," Applied Optics **18**, 712-723 (1979).
16. E. Organelli, G. Dall'Olmo, R. J. W. Brewin, G. A. Tarran, E. Boss, and A. Bricaud, "The open-ocean missing backscattering is in the structural complexity of particles," Nature Communications **9**(2018).
17. J. Gienger, H. Gross, V. Ost, M. Bar, and J. Neukammer, "Assessment of deformation of human red blood cells in flow cytometry: measurement and simulation of bimodal forward scatter distributions," Biomedical Optics Express **10**, 4531-4550 (2019).
18. A. A. Vinokurov, V. B. Il'in, and V. G. Farafonov, "ScattPy: A new Python package for light scattering computations," Journal of Quantitative Spectroscopy and Radiative Transfer **112**, 1733-1740 (2011).
19. H. Hillebrand, C. D. Durselen, D. Kirschtel, U. Pollingher, and T. Zohary, "Biovolume calculation for pelagic and benthic microalgae," Journal of Phycology **35**, 403-424 (1999).
20. B. D. Hobson and P. A. Sims, "Critical Analysis of Particle Detection Artifacts in Synaptosome Flow Cytometry," Eneuro **6**(2019).
21. J. R. Casey, K. M. Bjorkman, S. Ferron, and D. M. Karl, "Size dependence of metabolism within marine picoplankton populations," Limnology and Oceanography **64**, 1819-1827 (2019).
22. D. A. Bryant, "The beauty in small things revealed," Proceedings of the National Academy of Sciences **100**, 9647 (2003).
23. G. B. J. Dubelaar, J. W. M. Visser, and M. Donze, "Anomalous behavior of forward and perpendicular light-scattering of a cyanobacterium owing to intracellular gas vacuoles," Cytometry **8**, 405-412 (1987).
24. J. Peurifoy, Y. C. Shen, L. Jing, Y. Yang, F. Cano-Renteria, B. G. DeLacy, J. D. Joannopoulos, M. Tegmark, and M. Soljacic, "Nanophotonic particle simulation and inverse design using artificial neural networks," Science Advances **4**(2018).